1521-0103/352/1/77–89$25.00
THE JOURNAL OF PHARMACOLOGY AND EXPERIMENTAL THERAPEUTICS

http://dx.doi.org/10.1124/jpet.114.218131
J Pharmacol Exp Ther 352:77–89, January 2015

M1 Polarization Bias and Subsequent Nonalcoholic Steatohepatitis Progression Is Attenuated by Nitric Oxide Donor DETA NONOate via Inhibition of CYP2E1-Induced Oxidative Stress in Obese Mice[S]

Ratanesh Kumar Seth, Suvarthi Das, Sahar Pourhoseini, Diptadip Dattaroy, Stephen Igwe, Julie Basu Ray, Daping Fan, Gregory A. Michelotti, Anna Mae Diehl, and Saurabh Chatterjee

Environmental Health and Disease Laboratory, Department of Environmental Health Sciences, Arnold School of Public Health, University of South Carolina, Columbia, South Carolina (R.K.S., S.D., S.P., D.D., S.C.); School of Science, Technology, Engineering and Mathematics (STEM), Dillard University, New Orleans, Louisiana (S.I., J.B.R.); Department of Cell Biology and Anatomy, University of South Carolina School of Medicine, Columbia, South Carolina (D.F.); and Division of Gastroenterology, Duke University, Durham, North Carolina (G.A.M., A.M.D.)

Received July 14, 2014; accepted October 23, 2014

ABSTRACT

Activation of M1 macrophages in nonalcoholic steatohepatitis (NASH) is produced by several external or endogenous factors: inflammatory stimuli, oxidative stress, and cytokines are known. However, any direct role of oxidative stress in causing M1 polarization in NASH has been unclear. We hypothesized that CYP2E1-mediated oxidative stress causes M1 polarization in experimental NASH, and that nitric oxide (NO) donor administration inhibits CYP2E1-mediated inflammation with concomitant attenuation of M1 polarization. Because CYP2E1 takes center stage in these studies, we used a toxin model of NASH that uses a ligand and a substrate of CYP2E1 for inducing NASH. Subsequently, we used a methionine and choline–deficient diet-induced rodent NASH model where the role of CYP2E1 in disease progression has been shown. Our results show that CYP2E1 causes M1 polarization bias, which includes a significant increase in interleukin-1β (IL-1β) and IL-12 in both models of NASH, whereas CYP2E1-null mice or diallyl sulfide administration prevented it. Administration of gadolinium chloride ($GdCl_3$), a macrophage toxin, attenuated both the initial M1 response and the subsequent M2 response, showing that the observed increase in cytokine levels is primarily from macrophages. Based on the evidence of an adaptive NO increase, the NO donor administration in vivo that mechanistically inhibited CYP2E1 catalyzed the oxidative stress during the entire study in NASH-abrogated M1 polarization and NASH progression. The results obtained show the association of CYP2E1 in M1 polarization, and that inhibition of CYP2E1 catalyzed oxidative stress by an NO donor (DETA NONOate [(*Z*)-1-[*N*-(2-aminoethyl)-*N*-(2-ammonioethyl) amino]diazen-1-ium-1,2-diolate]) can be a promising therapeutic strategy in NASH.

Introduction

Nonalcoholic steatohepatitis (NASH) can be characterized by inflammation, hepatocyte necrosis, and often fibrosis (Bohinc and Diehl, 2012). If unchecked, NASH can rapidly progress to cirrhosis and hepatocellular carcinoma. To make matters worse, NASH treatment is further complicated by the absence of a proven treatment regimen owing to the silent nature of the disease and to patients reporting to clinics at an advanced stage (Cheung and Sanyal, 2009). The two-hit or multi-hit paradigms range from defective triglyceride production and release, free fatty acid content, oxidative stress, damage-associated molecular patterns, cytokine release, and more recently, xenobiotic enzymes, such as cytochrome P450 (Tilg and Moschen, 2008, 2010; Abdelmegeed et al., 2012, 2013). A recent report of the NASH rodent model coupled with several research studies on alcoholic steatohepatitis clearly ascribe the role of CYP2E1 in the generation of oxygen species, which can act as a second hit for the progression of

This work was supported by National Institutes of Health Pathway to Independence Award, National Institute of Environmental Health Sciences [Grant 4R00-ES019875-02] (to S.C.); and the National Institutes of Health National Institute of Diabetes and Digestive and Kidney Diseases [Grant R01-DK053792] (to A.M.D.).
dx.doi.org/10.1124/jpet.114.218131.
[S] This article has supplemental material available at jpet.aspetjournals.org.

ABBREVIATIONS: 1400W, *N*′-[[3-(aminomethyl)phenyl]methyl]ethanimidamide; BDCM, bromodichloromethane; CRN, National Institutes of Health Nonalcoholic Steatohepatitis Clinical Research Network; DAB, 3,3′-diaminobenzedine; DAS, diallyl sulfide; DETA NONOate, (*Z*)-1-[*N*-(2-aminoethyl)-*N*-(2-ammonioethyl)amino]diazen-1-ium-1,2-diolate; DAPI, 4′,6-diamidino-2-phenylindole; DIO, diet-induced obesity mouse model; ELISA, enzyme-linked immunosorbent assay; 4-HNE, 4-hydroxynonenal; 4-HNE-His, 4-hydroxynonenal-histidine; HRP, horseradish peroxidase; IL, interleukin; KO, knockout; MCD, methionine and choline–deficient; MCS, methionine and choline sufficient diet; NASH, nonalcoholic steatohepatitis; NO, nitric oxide; NOS, nitric oxide synthase; α-SMA, α-smooth muscle actin; V-PYRRO/NO, O_2-vinyl 1-(pyrrolidin-1-yl)diazen-1-ium-1,2-diolate.

NASH (Caro and Cederbaum, 2004; Aubert et al., 2011; Abdelmegeed et al., 2013). The second hit can couple the proinflammatory changes to the liver microenvironment and aid in the progression of severe end-stage NASH complications, which may include fibrosis and hepatocellular carcinoma.

Inflammation is central to NASH progression (Tilg and Moschen, 2008; Bohinc and Diehl, 2012; Ganz and Szabo, 2013). We previously showed that inflammation linked to oxidant stress is closely associated with NASH progression (Chatterjee et al., 2013; Das et al., 2013b; Seth et al., 2014). Hepatocyte necrosis, lipid peroxidation, and activation of purinergic receptor P2X7r can give rise to NADPH oxidase activation, leading to Kupffer cell activation, a key event in NASH progression (Chatterjee et al., 2013; Das et al., 2013a). Also, proinflammatory cytokine induction depended on oxidative stress and CYP2E1 in a toxin model of NASH (Das et al., 2013a). In a recent report, Sutti et al. (2014) showed that when mice were immunized with malonyldialdehyde adducted bovine serum albumin, it did not affect control mice livers, but it did further stimulate transaminase release, lobular inflammation, and the hepatic expression of proinflammatory cytokines in mice fed a methionine and choline–deficient (MCD) diet that exhibits NASH. The increased severity of NASH in the immunized MCD-diet mice involved liver recruitment of the T helper (T_H1) activation of CD41 T cells, which, in turn, further stimulated macrophage M1 responses (Sutti et al., 2014).

Though the rodent models of NASH have established the prominent role of CYP2E1 and its associated oxidative stress as key to NASH progression, the mechanisms of how CYP2E1 regulates inflammation, especially the polarization of macrophages and generation of a proinflammatory response, has been unclear.

Recent published reports indicate a strong M1 bias after the inflammatory trigger (Maina et al., 2012). M1 polarization is associated with higher levels of nitric oxide (NO), interleukin-1β (IL-1β), tumor necrosis factor-α, interferon-γ, IL-12, and several chemoattractants (Maina et al., 2012). This happens mostly in the initial phases of liver injury in rodent models, which have been used to study NASH progression. Patients with early phases of NASH occurrences also have reciprocated an M1 bias (Bertola et al., 2010). However, NASH progression is also associated with a delayed shift into profibrotic mechanisms, which might require an M2 polarization. Inflammatory surges in many diseases are accompanied by a late M2 shift, which can arise from higher proinflammatory cytokine levels, higher NO levels, or both (Liu et al., 2014). High NO levels have been accompanied by higher arginase activity, leading to release of transforming growth factor-β, IL-4, and IL-13, which are primarily anti-inflammatory but do contribute to the fibrotic process (Chatterjee et al., 2006; Liu et al., 2014). The role of higher NO levels in causing a feedback loop triggering anti-inflammatory mechanisms can be a potential therapeutic approach in NASH, given the use of an NO donor in a single study for NASH remediation involving ob/ob mice, the spontaneous knockout (KO) of leptin, where no mechanistic inputs were provided (de Oliveira et al., 2008). Along with studies of the boosting of NO levels are the extensive studies about the role of NO in inhibiting CYP2E1; the use of an NO donor to treat NASH can be an excellent regimen (Gergel et al., 1997; Aitken et al., 2008).

Based on the existing literature, we hypothesized that CYP2E1-mediated oxidative stress causes M1 polarization in experimental NASH and that NO donor administration inhibits CYP2E1-mediated oxidative stress and inflammation with concomitant attenuation of M1 polarization. Because CYP2E1 takes center stage in these studies, we used a toxin model of NASH that uses a ligand and a substrate of CYP2E1 for inducing NASH; subsequently, we used an MCD diet–induced rodent NASH model in which the role of CYP2E1 in its progression has been shown. Our results show that CYP2E1 causes M1 polarization bias in both models of NASH, but it is prevented in the CYP2E1-null mouse model. NO donor administration inhibits CYP2E1 mRNA, CYP2E1-induced oxidative stress, M1 polarization, and NASH progression.

Materials and Methods

Bromodichloromethane (BDCM), gadolinium chloride ($GdCl_3$), and corn oil were purchased from Sigma-Aldrich (St. Louis, MO). DETA NONOate [(*Z*)-1-[*N*-(2-aminoethyl)-*N*-(2-ammonioethyl)amino]diazen-1-ium-1,2-diolate] was purchased from Cayman Chemical (Ann Arbor, MI). Diallyl sulfide (DAS) was purchased from Santa Cruz Biotechnology (Santa Cruz, CA). Anti–4-hydroxynonenal (4-HNE), anti–IL-1β, anti–IL-13, anti-CYP2E1 and anti–α-smooth muscle actin (α-SMA) primary and secondary antibodies conjugated with horseradish peroxidase (HRP) were purchased from Abcam (Cambridge, MA). Anti–IL-12 antibody was purchased from Pierce Biotechnology (Rockford, IL). Secondary antibodies conjugated with fluorophore (AlexaFluor 633) were purchased from Life Technologies (Carlsbad, CA). The Nitric Oxide Fluorometric Assay Kit was purchased from BioVision Incorporated (Milpitas, CA). The nitric oxide synthase type 2 (NOS2) inhibitor, 1400W (*N*′-[[3-(aminomethyl)phenyl]methyl] ethanimidamide), was purchased from Cayman Chemical. HNE-histidine (HNE-His) Adduct ELISA Kit (enzyme-linked immunosorbent assay) was purchased from Cell Biolabs (San Diego, CA). All experimental wild-type and gene-specific KO mice were purchased from The Jackson Laboratories (Bar Harbor, ME). Animal diets were purchased from Research Diets (New Brunswick, NJ). All other chemicals were of analytical grade and were purchased from Sigma-Aldrich unless otherwise specified.

Mouse Models

All mice had ad libitum access to food and water and were housed in a temperature-controlled room at 23–24°C with a 12-hour light/dark cycle. All animals were treated in strict accordance with the NIH Guide for the Humane Care and Use of Laboratory Animals and local International Animal Care and Use Committee standards. The study was approved by the institutional review board both at Duke University and the University of South Carolina at Columbia. After completion of the treatment, mice of all study groups were sacrificed for liver tissue and serum for the further experiments.

Mouse Model for Toxin-Induced NASH. Pathogen-free, male, C57BL/6J background mice were used as wild-type mice for diet-induced obesity model (DIO). Mice that contained the deleted CYP2E1 gene (129/Sv-*Cyp2e1*^{tm1Gonz}/J) (CYP2E1 KO) and that contained the deleted *NOS2* gene (B6.129P2-Nos2^{tm1Laul}/J) (NOS2 KO) were fed with a high-fat diet and treated identically to the DIO mice. The mice were housed one per cage before any experimental use were and fed with a high-fat diet (60% kcal) from 6 to 16 weeks.

Administration of BDCM-Induction of Liver Injury. DIO mice and high-fat diet–fed gene-specific KO mice at 16 weeks were administered BDCM (1.0 mmol/kg, diluted in corn oil) intraperitoneally, twice a week for 1 week to assess the early stage of liver injury (DIO + BDCM, 1 week) and for 4 weeks to assess the effects of chronic exposure of BDCM (DIO + BDCM, 4 weeks). DIO mice and high-fat diet–fed gene-specific KO mice treated with corn oil (vehicle control of BDCM) were used as controls.

Mouse Model for Diet-Induced NASH. Pathogen-free, male, C57BL/6J background, wild-type mice were fed an MCD diet and were used as models for diet-induced NASH. Mice were fed with an MCD diet from 8 to 12 weeks of age, and the harvested livers were used to study early-stage liver injury (MCD, 4 weeks). Livers from mice fed with an MCD diet from 8 to 16 weeks of age were used to study late-stage liver injury (MCD, 8 weeks). Additionally, one set of wild-type mice fed with a methionine and choline–sufficient diet (MCS; control diet for MCD) was used as a control.

Administration of DETA NONOate, an NO Donor, and 1400W. DIO mice at 16 weeks were given BDCM and treated with DETA NONOate (1.0 mg/kg diluted in phosphate-buffered saline) 1 hour before each administration of BDCM for 1 week (DIO + BDCM + NO, 1 week) and for 4 weeks (DIO + BDCM + NO, 4 weeks). The MCD diet–fed mice were given DETA NONOate twice a week intraperitoneally from 8 to 12 weeks of age (MCD + NO, 4 weeks) and from 8 to 16 weeks of age (MCD + NO, 8 weeks). We administered 1400W intraperitoneally, as described elsewhere (Chatterjee et al., 2013).

Inhibition of CYP2E1 by DAS (CYP2E1 Inhibitor). Another set of MCD diet–fed mice were treated with 50 mg/kg DAS (diluted in corn oil) twice a week intraperitoneally from 8 to 12 weeks of age (MCD + DAS, 4 weeks) and from 8 to16 weeks of age (MCD + DAS, 8 weeks) (Hu et al., 1996).

Macrophage Depletion by $GdCl_3$. DIO mice at 16 weeks of age were given BDCM and were injected with $GdCl_3$ (10 mg/kg) intravenously 24 hours before BDCM exposure (Chatterjee et al., 2013).

Laboratory Analyses

Immunohistochemistry. Formalin-fixed, paraffin-embedded liver tissue from all mice groups were cut into 5-μm-thick tissue sections. Each section was deparaffinized using standard protocol as described by Seth et al. (2013). Epitope retrieval of deparaffinized sections was performed using an epitope retrieval solution and steamer (IHC World, Woodstock, MD) following the manufacturer's protocol. Endogenous peroxidases were blocked using 3% H_2O_2 for 5 minutes. After blocking with 5% normal serum, the tissue sections were incubated with primary antibodies: 1) anti–4-hydroxynonenal and 2) anti–α-smooth muscle actin (diluted to 1:500). Species-specific anti-IgG secondary antibodies and conjugation with HRP were performed using Vectastain Elite ABC kit (Vector Laboratories, Burlingame, CA) following the manufacturer's protocols. We used 3,3′-diaminobenzedine (DAB) as a chromogen substrate. Sections were counterstained with Mayer's hematoxylin. Washing with phosphate-buffered saline containing 0.05% Tween 20 was performed three times between the steps. Sections were mounted in the water-based mounting media Simpo Mount (GBI Laboratories, Mukilteo, WA) and were observed under 10×/20× objective magnification. Morphometric analysis was performed using cellSens software from Olympus America (Center Valley, PA).

Immunofluorescence Microscopy. Paraffin-embedded liver tissue from all the mouse groups was cut into 5-μm-thick sections. Each section was deparaffinized using a standard protocol. Heat-based epitope retrieval of deparaffinized sections was performed using an epitope retrieval solution and steamer following the manufacturer's protocol. The sections were treated with 0.01% triton X-100 before blocking with 5% normal serum. The primary antibodies 1) anti–IL-1β, 2) anti–IL-12, and 3) anti–IL-13 were used in 1:200 dilutions and incubated overnight at 4°C. Species-specific anti-IgG secondary antibody conjugated with Alexa Fluor 633 was used to observe the antigen-specific immunoreactivity in the red channel. Sections were mounted in ProLong gold antifade reagent (Life Technologies) with 4′,6-diamidino-2-phenylindole (DAPI). Images were taken under 20× objective magnification using an Olympus BX51 microscope (Olympus America).

Quantitative Real-Time Polymerase Chain Reaction. Gene expression levels in tissue samples were measured by two-step quantitative real-time polymerase chain reaction. A standard protocol as described by Seth et al. (2013) was used to extract the total RNA from liver tissues and to prepare cDNA from RNA extracts. We performed quantitative real-time polymerase chain reaction with gene-specific forward and reverse primers using SsoAdvanced universal SYBR Green supermix (Bio-Rad Laboratories, Hercules, CA) and a CFX96 thermal cycler (Bio-Rad Laboratories). The threshold cycle values for the selected genes were normalized against 18S (internal expression control) value in the same sample. Each reaction was performed in triplicate for each gene and for each tissue sample. DIO mouse liver samples were used as the control for comparison with all other liver samples in the toxin-induced NASH group; an MCS-diet mouse liver sample was used as control for comparison with all other liver samples of the diet-induced NASH group. The relative fold change was calculated by using CFX Manager software (Bio-Rad Laboratories). The sequences for the primers used for real-time PCR are provided in Table 1 in 5′ to 3′ orientation.

Western Blot. We homogenized 25 mg of tissue from each liver sample in 150 μl of radioimmunoprecipitation assay buffer with protease inhibitor (1×) (Pierce Biotechnology) using a Dounce homogenizer. The homogenate was centrifuged, and the supernatant was collected and saved for experimental use. From each homogenate, 30 μg of denatured protein was loaded per well of Novex 4%–12% Bis-Tris Gradient Gel (Life Technologiesand was subjected for SDS-PAGE. Protein bands were transferred to nitrocellulose membranes using precut nitrocellulose/filter paper sandwiches (Bio-Rad Laboratories) and the Trans-Blot Turbo transfer system (Bio-Rad Laboratories). Blots were blocked with 5% nonfat milk solution. Primary antibodies against CYP2E1 and β-actin were used at recommended dilutions. Species-specific anti-IgG secondary antibodies conjugated with HRP were used. Pierce ECL Western Blotting substrate (ThermoFisher Scientific, Rockford, IL) was used. The blot was developed using BioMax MS Films and cassettes (with intensifying screen (Eastman Kodak Company, Rochester, NY). The images were subjected to densitometry analysis using Laboratory Image 2006 Professional 1D gel analysis software from Kapelan Bio-Imaging Solutions (Liepzig, Germany).

ELISA. Immunoreactivity for 3-nitrotyrosine was detected in liver homogenates using standard ELISA (Chatterjee et al., 2009). Briefly, a polystyrene, high-binding, 96-well plate was coated with 5 μg of each protein. The wells were blocked with 5% nonfat milk. Primary antibody, anti–3-nitrotyrosine (1:1000 dilution), was used. Species-specific

TABLE 1
Primers used for quantitative real-time polymerase chain reaction (5′ to 3′ orientation)

Gene	Primer Sequence
IL-1β	Sense: CCTCGGCCAAGACAGGTCGC Antisense: TGCCCATCAGAGGCAAGGAGGA
IL-12	Sense: GCTTCTCCCACAGGAGGTTT Antisense: CTAGACAAGGGCATGCTGGT
IL-23	Sense: AAAGGATCCGCCAAGGTCTG Antisense: GCAGGCTCCCCTTTGAAGAT
Dectin-1	Sense: AGGGAGCCACCTTCTCATCT Antisense: CTTCACCTTGGAGGCCCATT
IL-4	Sense: CATCGGCATTTTGAACGAG Antisense: CGAGCTCACTCTCTGTGGTG
IL-13	Sense: CACACAAGACCAGACTCCCC Antisense: TCTGGGTCCTGTAGATGGCA
CYP2E1	Sense: GGCGCATCGTGGTCCTGCAT Antisense: CCGCACGTCCTTCCATGTGGG
α-SMA	Sense: GGAGAAGCCCAGCCAGTCGC Antisense: ACCATTGTCGCACACCAGGGC

anti-IgG secondary antibody conjugated with HRP was used. TMB Substrate Solution (Pierce Biotechnology) was used to develop color. To stop the reaction, we used 2 N sulfuric acid. The plate was read at 450 nm using a Synergy HT plate reader (BioTek Instruments, Winooski, VT). Immunoreactivity of the HNE-His adduct was detected in liver homogenate using the OxiSelect HNE-His adduct ELISA kit (Cell Biolabs) following the manufacturer's protocol.

Histopathology. Formalin-fixed liver sections were stained with H&E as per standard protocol and were observed under the light microscope using 10× objective magnification. The fibrotic stage of the liver tissue was evaluated by staining collagen deposition in liver sections using Sirius Red. The Picrosirius Red staining of liver sections was performed by using a NovaUltra Sirius Red stain kit following the manufacturer's protocol (IHC World).

Statistical Analyses

All in vivo experiments were repeated three times with three mice per group (data from each group of three mice were pooled). All experiments were repeated three times, and the statistical analysis was performed by analysis of variance, including the morphometric analysis followed by the Bonferroni post hoc correction for intergroup comparisons. Quantitative data from mRNA expression as depicted by the relative fold change were analyzed via Student's t test. For all analyzes, $P < 0.05$ was considered statistically significant.

Results

Lipid Peroxidation and Tyrosyl Radical Formation in NASH Progression Is Associated with the Presence of Hepatic CYP2E1. To study the nature of the oxidative species generated as a result of CYP2E1 activity in models of NASH, 4-HNE-His adducts and 3-nitrotyrosine adducts were estimated by ELISA. Results showed that the DIO + BDCM group had statistically significantly increased 4-HNE-His adducts at 1 week after initiation of the study as compared with the DIO group ($^*P < 0.05$) (Fig. 1A). Mice that were deficient in the CYP2E1 gene had significantly decreased 4-HNE-His adducts as compared with the DIO + BDCM group at the same time point (Fig. 1A).

Because we used the toxin BDCM, which is known to produce dihalomethyl radicals after its reactivity with CYP2E1, we used another commonly used dietary NASH model, the methionine and choline–deficient diet, for evaluating the role of oxidative stress induced by CYP2E1. The results showed that 4-HNE-His adducts were statistically significantly high in the MCD group as compared with the MCS control group at 4 weeks (comparable to 1 week in the DIO model) ($P < 0.05$) (Fig. 1A). The MCD-diet mice, when treated with the CYP2E1 inhibitor DAS, had significantly decreased 4-HNE-His adducts, suggesting that CYP2E1 is necessary for the generation of 4-HNE-His adducts, a direct consequence of lipid peroxidation in the liver (Fig. 1A). Earlier work with CYP2E1 had suggested that the enzyme can produce superoxide radicals based on its strong NADPH oxidase-like activity (Gergel et al., 1997). Similarly, Gergel et al. (1997) showed that O_2^- can react with NO to produce $ONOO^-$. Based on its ability to produce $ONOO^-$, we studied the generation of 3-nitrotyrosine adducts in both toxin-treated DIO mice and MCD-diet mouse livers. Our results showed that 3-nitrotyrosine adduct levels were statistically significantly increased in the DIO + BDCM group as compared with the DIO-only group at 1 week ($^*P < 0.05$) (Fig. 1B). The absence of the CYP2E1 gene significantly decreased 3-nitrotyrosine adducts as compared with the DIO + BDCM group at the same time point ($P < 0.05$) (Fig. 1B). The MCD-diet mice at 1 week had similarly higher 3-nitrotyrosine adducts when compared with the control-diet mice ($P < 0.05$), whereas the MCD-diet mice that were treated with DAS had a significant decrease in the 3-nitrotyrosine adduct formation (Fig. 1B), though a significant decrease in tyrosyl radical formation was not observed at 4 weeks.

Our results suggest that CYP2E1 activity in NASH generates nitro-tyrosyl radicals probably through peroxynitrite formation from high CYP2E1-induced O_2^-, at least in the diet + toxin model of NASH. However, it is interesting that CYP2E1-induced 4-HNE can also generate O_2^-, thus producing tyrosyl radical formation and 3-nitrotyrosine adducts (Whitsett et al., 2007).

Figure 1C shows the localization of the immunoreactivity of 4-HNE in the livers of rodent NASH models. We found that 4-HNE immunoreactivity was mainly localized in the zone 3 (centrilobular) regions of livers in the BDCM model of NASH (Fig. 1Ci–iii), whereas the 4-HNE immunoreactivity was uniformly higher in the centrolobular and periportal areas of livers from the MCD-diet model of NASH. An absence of CYP2E1 enzyme (CYP2E1 KO) or administration of the CYP2E1 inhibitor DAS significantly decreased the 4-HNE immunoreactivity in the NASH livers of both models ($P < 0.05$) (Fig. 1, C and D). Nonavailability of a direct assay method that would only specifically estimate CYP2E1 activity from tissue homogenates led us to indirectly rely on CYP2E1-induced oxidative radical formation as an index for assessing its catalytic role in the models of NASH being used in this study. BDCM is a hepatotoxin and is metabolized by CYP2E1 by forming dihalomethyl radicals, as shown by Tomasi et al. (1985).

CYP2E1-Mediated Oxidative Stress Is Associated with M1 Polarization Bias in NASH Livers. Recent evidence involving morbidly obese patients with NASH etiology has been strongly associated with a specific increase in the liver expression of a wide array of proinflammatory M1 cytokines, especially IL-1β (Bertola et al., 2010). Recent reports from our laboratory have shown that CYP2E1-induced oxidative stress causes up-regulation of pattern recognition receptor P2X7r (purinergic receptor X7), which has a direct role in activation of T_H1 cells (Das et al., 2013b). CYP2E1-null mice also have lower F4/80-positive cells, which are primarily macrophages, followed by levels of intrahepatic tumor necrosis factor-α and monocyte chemoattractant protein 1 as compared with wild-type mice that have NASH (Abdelmegeed et al., 2012). To study the patterns of macrophage activation and M1 polarization bias in NASH, we estimated the intrahepatic M1 cytokine levels of IL-1β, IL-12, IL-23, and Dectin-1. Because macrophages play a distinct role in the polarization, we administered the macrophage toxin $GdCl_3$ to deplete the residential and infiltrating macrophages in the liver only in the toxin model of NASH to show the mechanistic role of the macrophages (Chatterjee et al., 2013).

NASH develops over a period of time and is progressive in nature. An early phase of sinusoidal injury and inflammation has been reported for most models of NASH (Pasarin et al., 2012). For the toxin (DIO + BDCM) model of NASH, we used a 1-week time point for measuring M1 phenotypic shift and inflammation, but we used 4 weeks for the MCD model because this model extends for 8 weeks. Our results showed that mRNA expression of IL-1β, IL-12, 1L-23, and Dectin-1 was significantly upregulated in the DIO + BDCM group as

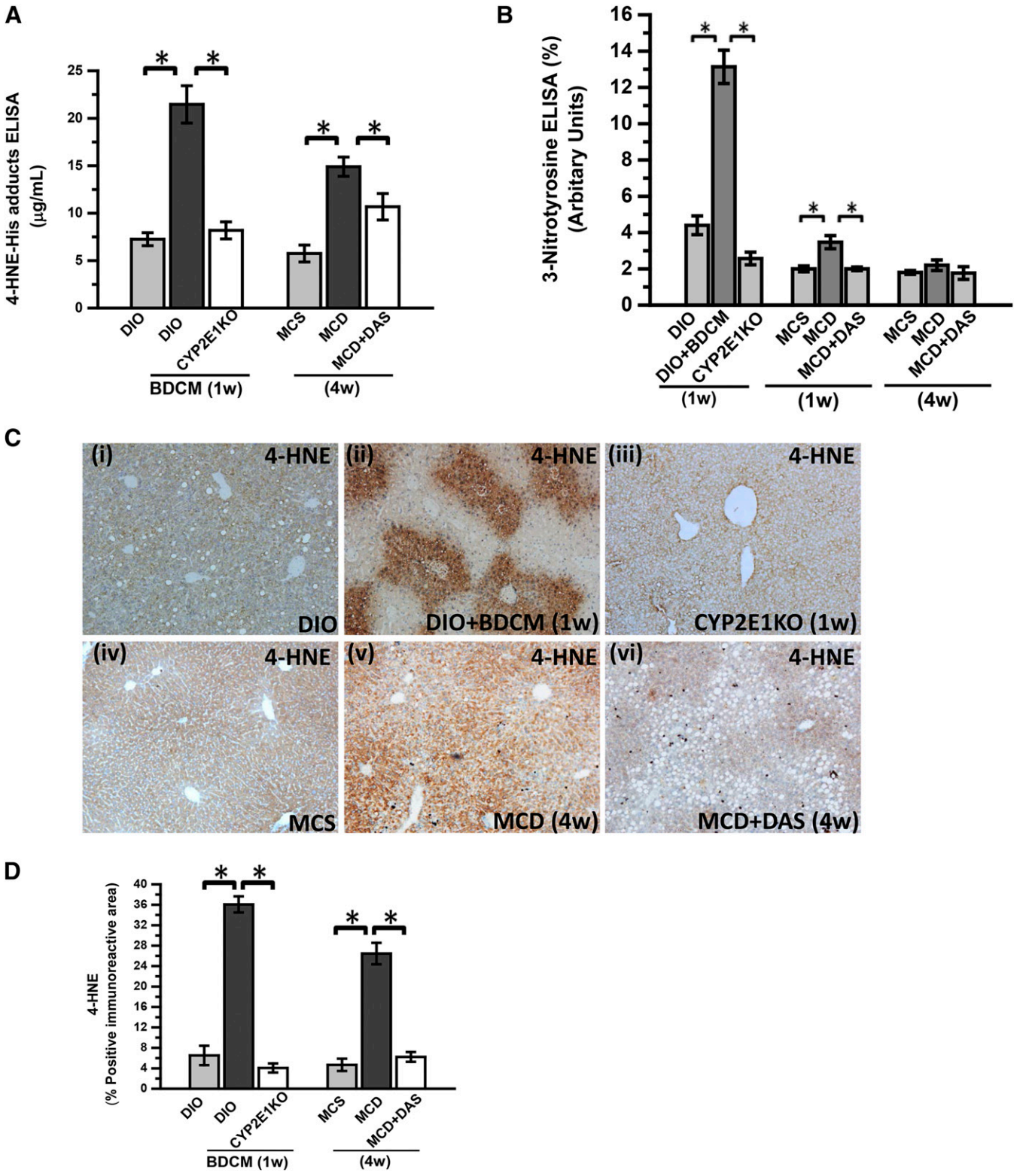

Fig. 1. BDCM exposure in DIO mice and MCD diet wild-type mice generates CYP2E1-mediated oxidative stress. (A) Quantification of 4-HNE-His adducts (stable adducts of 4-HNE) in mouse liver homogenate by indirect ELISA of DIO mice, DIO mice exposed to BDCM for 1 week (DIO + BDCM, 1 week), mice with the CYP2E1 gene deleted exposed to BDCM (CYP2E1 KO), mice fed a MCS diet, mice fed a MCD diet, and mice fed a MCD diet and treated with diallyl disulfide (CYP2E1 inhibitor) for 4 weeks (MCD + DAS). The *y*-axis represents the 4-HNE-His adduct in pg/ml ($n = 3$). *$P < 0.05$ is considered statistically significant. (B) Indirect ELISA of 3-nitrotyrosine in mouse liver homogenate of DIO, DIO + BDCM (1 week), CYP2E1 KO, MCS, MCD, and MCD + DAS (1 week and 4 weeks). The *y*-axis represents the percentage levels of 3-nitrotyrosine immunoreactivity ($n = 3$). *$P < 0.05$ is considered statistically significant. (C) Immunohistochemistry of mouse liver slices depicting 4-HNE immunoreactivity (lipid peroxidation) in DIO, DIO + BDCM (1 week), CYP2E1 KO, MCS, MCD, and MCD + DAS. Magnification: 10× ($n = 3$). (D) Morphometric analysis of 4-HNE immunoreactivity. The *y*-axis shows the percentage of the positive immunoreactive area ($n = 3$, analysis of images from three separate microscopic fields). *$P < 0.05$ is considered statistically significant.

compared with the DIO-only group ($P < 0.05$) (Fig. 2A). CYP2E1-null mice or mice that were treated with $GdCl_3$ had statistically significantly lower M1 cytokine levels as compared with the DIO + BDCM group ($P < 0.05$) (Fig. 2A). Similar trends were seen in the MCD model of NASH where IL-1β, IL-12, IL-23, and Dectin-1 mRNA were statistically significantly upregulated in the early phase of NASH progression (4 weeks of the MCD diet) ($P < 0.05$) (Fig. 2B).

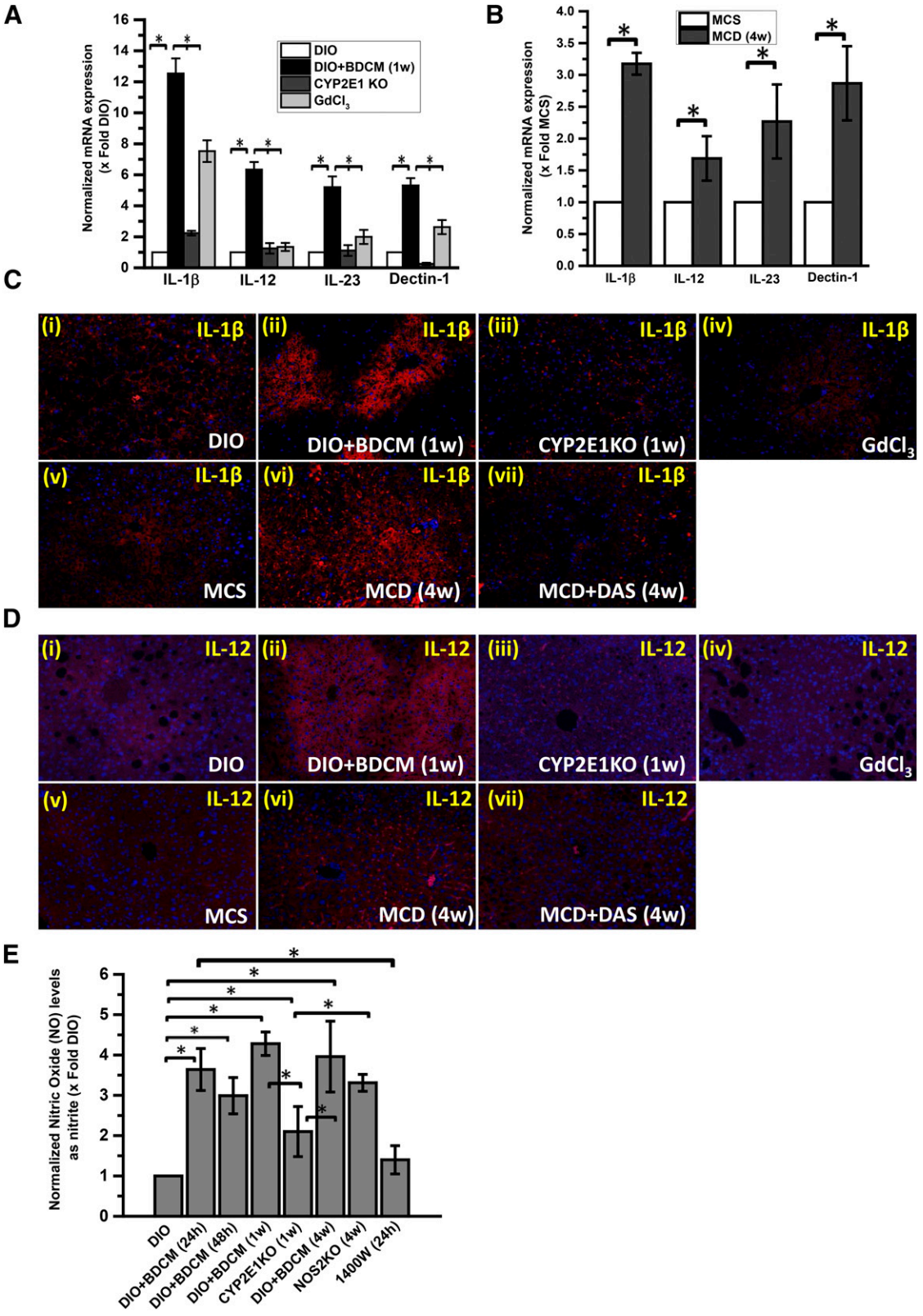

Fig. 2. M1 polarization depends on oxidative stress mediated by CYP2E1 activity. (A) Quantitative real-time polymerase chain reaction analysis of liver IL-1β, IL-12, IL-23, and Dectin-1 mRNA expression of DIO, DIO + BDCM (1 week), CYP2E1 KO, and $GdCl_3$-treated (macrophage-depleted) mice. The

To characterize the localization of M1 cytokines in the liver, we performed immunofluorescence microscopy on liver slices from both the toxin model and MCD-diet model of NASH. Our results showed that IL-1β and IL-12 showed higher immunoreactivity in the DIO + BDCM and MCD groups as compared with their controls (DIO and MCS, respectively) (Fig. 2, C and D), whereas the $GdCl_3$- and DAS-treated groups had significantly lower immunoreactivity for both IL-1β and IL-12 (Fig. 2, C and D).

We measured NO in the form of nitrite from tissue homogenates (Fig. 2E). Our results showed that the NO levels were significantly higher in the DIO + BDCM group at 24 hours, 1 week, and 4 weeks, while use of CYP2E1-null mice decreased the NO levels significantly (Fig. 2E). Use of 1400W decreased the NO levels at 24 hours. Use of NOS2 KO mice did not significantly decrease the NO levels as compared with the DIO + BDCM group, suggesting the involvement of other NOS, especially NOS3 (Fig. 2E).

These data clearly show that CYP2E1-induced oxidative stress might play a role in causing the NASH liver to shift toward M1 type polarization bias. Further, the decrease in NO levels after 1400W-treatment (a specific NOS2 inhibitor) in the early (24-hour) phase of NASH in mice and the resistance to a decrease in NOS2 KO mice at later stages show that NOS2 may be involved in the early stage of NASH progression, whereas other NOS isoforms, especially NOS3, may contribute to the increased NO levels at the late stages of the disease, probably owing to an adaptive response in the liver.

M2 Phenotypic Cytokine Release in Late NASH Stages Are Macrophage Dependent. NASH is likely associated with a significantly prolonged anti-inflammatory phase, which is predicted to originate from the initial M1 phase and can be shifted toward an M2 phenotype (Copaci et al., 2006). Several lines of evidence show that IL-10 and IL-13 (and IL-4 in some models) in NASH are increased in the late stages of progression, as reported by Shimamura et al. (2008). M2 cytokines, especially IL-4 and IL-13, were significantly elevated in fibrosis mediated by carbon tetrachloride (CCl_4) in the liver, a feature that is linked to end-stage NASH (Shimamura et al., 2008). To show the later M2 polarization shift, we studied the M2 cytokine profiles in our models of NASH. Our results showed that IL-4 and IL-13 were significantly elevated in mice that were coexposed to the hepatotoxin BDCM and the high-fat diet (Fig. 3A) ($P < 0.001$). Interestingly, the mRNA levels of these cytokines were significantly downregulated in the MCD model of NASH (Fig. 3B). Depletion of macrophages by $GdCl_3$ significantly blunted the M2 phenotypic response (Fig. 3A) ($P < 0.05$), suggesting a direct link with the macrophage response in M2 phenotype bias. This observation holds true because the M1 phenotypic response was also blunted in these mice after $GdCl_3$ administration. Surprisingly, IL-4 and IL-13 mRNA expression was significantly decreased in the MCD model of NASH at 8 weeks (Fig. 3B). The IL-13 protein was significantly increased in both the models of NASH, as evidenced by IL-13 immunoreactivity in the centrilobular areas of the liver in the toxin model and periportal regions of the MCD model (Fig. 3C). Liver slices from the $GdCl_3$ administration model showed decreased immunoreactivity to IL-13, suggesting the strong link with the M2 phenotypic shift in late-stage NASH (4 weeks for the toxin model and 8 weeks for the MCD model of NASH) (Fig. 3C).

NO Donor Administration Attenuates CYP2E1-Induced M1 Cytokine Production. As evidenced by both preclinical and clinical studies, T_H1 polarization is an established phenomenon in early stage of NASH, but there is sparse evidence of an M1 phenotype bias except for the Kupffer cell M1/M2 transitions reported by Fukushima et al. (2009), Maina et al. (2012), and Zhou et al. (2014). Having established the role of CYP2E1-induced M1 polarization bias in both the toxin-induced high-fat diet and MCD models of NASH, we studied whether NO donor administration attenuated the M1 polarization phenotype in both models. The role of NOS and the generation of NO in the liver have not been studied with great detail. Studies by Fujita et al. (2010) show the direct involvement of NO in the development and progression of NASH. They hypothesized, based on the published studies, that increased NO may be contributing to excess nitrotyrosine, and hence, increasing oxidative-nitrosative stress in the liver (Fujita et al., 2010). Ajamieh et al. (2012) reported that atorvastatin conferred 70%–90% hepatic protection in NASH. The increased expression of Toll-like receptor-4 and activation of nuclear factor-κB were abrogated by the administration of atorvastatin, which was found to activate endothelial NOS (eNOS/NOS3) (Ajamieh et al., 2012). Prevention and reversion of nonalcoholic steatohepatitis in ob/ob mice by *S*-nitroso-*N*-acetylcysteine treatment has been reported in leptin deficient mice (ob/ob), but there was no mechanistic insight about the protection seen (de Oliveira et al., 2008).

Our own results, as reported in Fig. 2E, showed that increased NO response was not due to a proinflammatory NOS2-based response, and yet it can be justifiably assumed that it might be an adaptive response to liver injury. Based on this evidence, we studied the role of NO donor DETA NONOate on the corresponding M1 polarization-induced cytokine production and NASH progression. We attempted to study the early time points where we hypothesized polarization-induced cytokine induction to occur (1 week for the toxin model and 4 weeks for the MCD model). Our results showed that mRNA levels of M1 markers IL-1β, IL-12, IL-23, and Dectin-1 were significantly decreased in the group given NO donor and cotreated with a high-fat diet and toxin BDCM

y-axis represents the mRNA fold expression when normalized against the DIO-only group ($n = 3$). *$P < 0.05$ is considered statistically significant. (B) qRTPCR analysis of liver IL-1β, IL-12, IL-23, and Dectin-1 mRNA expression of MCS diet and MCD diet mice. The *y*-axis represents the fold of mRNA expression when normalized against MCS-only group ($n = 3$). *$P < 0.05$ is considered statistically significant. (C) Immunofluorescence images of IL-1β immunoreactivity (red), counterstained with DAPI (blue) of paraffin-embedded liver sections from (i) DIO, (ii) DIO + BDCM (1 week), (iii) CYP2E1KO, (iv) $GdCl_3$, (iv) MCS, (vi) MCD, and (vii) MCD + DAS. Magnification: 20× ($n = 3$). (D) Immunofluorescence images of IL-12 immunoreactivity (red), counterstained with DAPI (blue) of paraffin-embedded liver sections from (i) DIO, (ii) DIO + BDCM (1 week), (iii) CYP2E1 KO, (iv) $GdCl_3$, (v) MCS, (vi) MCD, and (vii) MCD + DAS. Magnification: 20× ($n = 3$). (E) NO levels measured as total nitrite (nitrite and nitrate converted to nitrite) by fluorometric assay in liver homogenates of DIO, DIO mice exposed to BDCM (DIO + BDCM) for 24 hours, DIO + BDCM for 48 hours, DIO + BDCM for 1 week, DIO + BDCM for 4 weeks, NOS2 (inducible) gene-deleted mice, mice given 1400W and exposed to BDCM for 24 hours, and NOS2 KO + BDCM for 4 weeks. The *y*-axis represents the fold of NO levels when normalized against the DIO-only group ($n = 3$). *$P < 0.05$ is considered statistically significant.

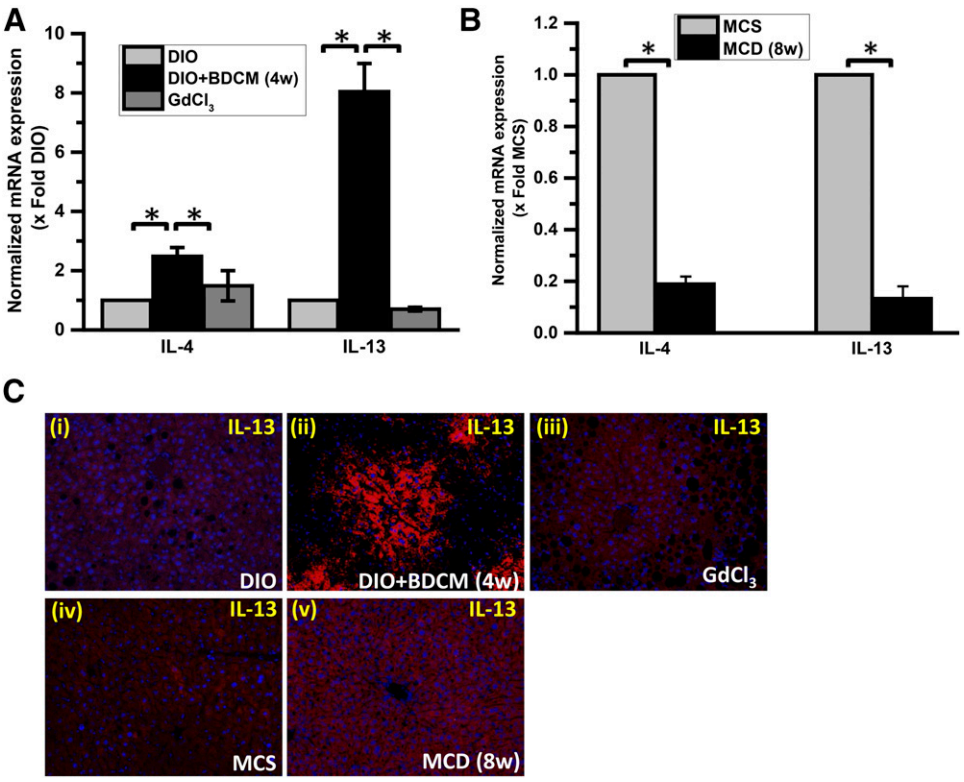

Fig. 3. Chronic exposure of BDCM leads to late M2 phenotypic shift. (A) quantitative real-time polymerase chain reaction (qRT-PCR) analysis of liver IL-4 and IL-13 mRNA expression in mice treated with DIO, DIO + BDCM (4 weeks), and $GdCl_3$. The *y*-axis represents the fold of mRNA expression when normalized against the DIO-only group ($n = 3$). *$P < 0.05$ is considered statistically significant. (B) qRT-PCR analysis of liver IL-4 and IL-13 mRNA expression of MCS diet and MCD diet mice. The *y*-axis represents the fold of mRNA expression when normalized against the MCS-only group, $n = 3$. *$P < 0.05$ is considered statistically significant. (C) Immunofluorescence images of IL-13 immunoreactivity (red), counterstained with DAPI (blue) of paraffin embedded liver sections from (i) DIO, (ii) DIO + BDCM (4 weeks), (iii) $GdCl_3$, (iv) MCS, and (v) MCD. Magnification: 20× ($n = 3$).

(as a second hit) (Fig. 4A) (*$P < 0.05$). Surprisingly, the MCD + NO-donor group showed a statistically significant increase in mRNA levels of the earlier described M1 markers as compared with MCD-only group (Fig. 4B) (*$P < 0.05$). Prominent M1 markers, IL-1β, IL-12, IL-23, and Dectin-1, had a significant increase in their mRNA patterns; based on their crucial roles in disease pathology, IL-1β and IL-12 were then assessed by immunofluorescence microscopy for their protein levels and localization (Fig. 4, C and D). The results showed that there was a visible decrease in IL-1β levels in NO donor groups of both models of NASH as compared with the respective BDCM-treated or MCD-diet mice groups (Fig. 4, C and D). These results suggest that there may be an interesting contrast between the mRNA profiles of the M1 markers in both models, but their protein profiles were found to be similar (a decrease in M1 markers) after NO donor administration in both models of NASH.

NO Donor Administration Attenuates M1 Polarization via Blockage of CYP2E1 Protein-Induced Oxidative Stress. Pioneering studies by Gergel et al. (1997) showed that NO could inhibit CYP2E1 activity and oxygen radical formation. The liver-selective NO donor, O_2-vinyl 1-(pyrrolidin-1-yl)diazen-1-ium-1,2-diolate (V-PYRRO/NO), protects HepG2 cells against CYP2E1-dependent toxicity (Gong et al., 2004). Based on this strong argument, we studied the mechanism of attenuation of M1 polarization by DETA NONOate.

Our results showed that administration of NO donor significantly decreased the mRNA levels of CYP2E1 at 1 week after cotreatment with toxin and high-fat diet (termed as the initial phase) as compared with the DIO + BDCM group alone (*$P < 0.05$) (Fig. 5A). Surprisingly, the mRNA levels of CYP2E1 were statistically significantly increased in the MCD model of NASH after NO donor administration (Fig. 5B) (*$P < 0.05$). Western blot analysis of the CYP2E1 protein showed no significant change in the liver levels of the protein in either of the two models except in CYP2E1-null mice (Fig. 5C).

Because NO donor has been shown to inhibit CYP2E1 activity and we could not identify a direct assay system to quantify CYP2E1 activity from liver homogenates, we resorted to the CYP2E1-induced lipid peroxidation as an index of CYP2E1 activity. ELISA and immunohistochemistry were used to quantify the lipid peroxidation product 4-HNE-His adducts after NO donor administration. Our results showed that there was a significant decrease in 4-HNE-His adducts in NO donor administered group as compared with the DIO + BDCM group at 1 week after study initiation, a time point when both increased oxidative stress and M1 polarization were observed (Fig. 5D) (*$P < 0.05$). These results were also observed in MCD model of NASH coadministered with NO donor. The NO donor group of MCD-diet mice had a statistically significant decrease in 4-HNE-His adducts as compared with the MCD group (Fig. 5D) (*$P < 0.05$).

Immunoreactivity to 4-HNE the lipid peroxidation product was also statistically significantly decreased in NO donor group for both the BDCM model and the MCD model of NASH (Fig. 5, E and F) (*$P < 0.05$). These results strongly suggested that NO donor administration significantly decreased CYP2E1-induced oxidative stress, which has been shown to be directly correlated to M1 polarization and NASH progression.

Our conclusions were strengthened by supplemental data provided by serum alanine aminotransferase and high-mobility group protein B1 mRNA expressions. The results

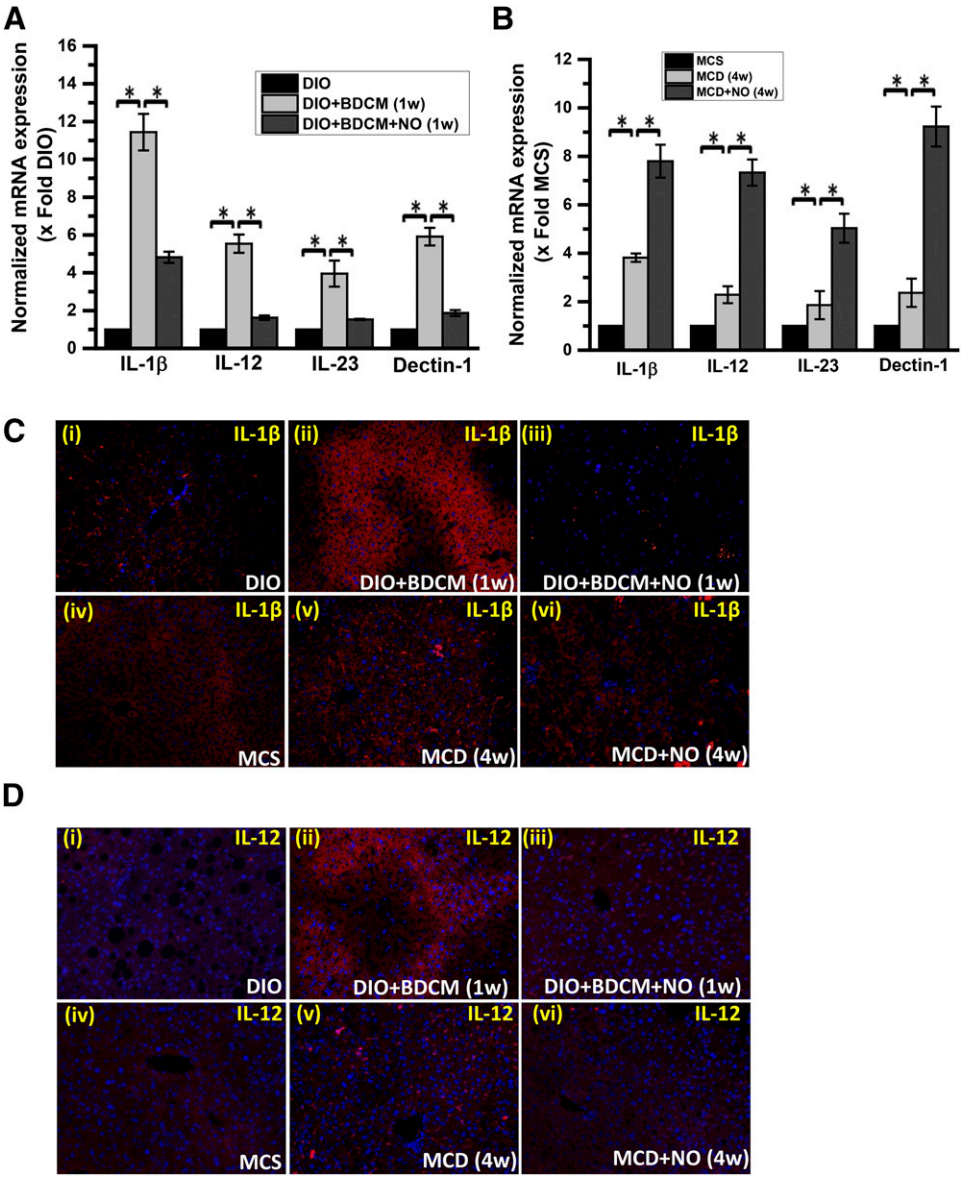

Fig. 4. NO donor DETA NONOate attenuates the CYP2E1-mediated M1 polarization bias. (A) mRNA expression analysis by quantitative real-time polymerase chain reaction (qRT-PCR) of liver IL-1β, IL-12, IL-23, and Dectin-1 from DIO mice, DIO + BDCM (1 week) mice, and DIO mice exposed to BDCM and treated with DETA NONOate (DIO + BDCM + NO) for 1 week. The y-axis represents the fold of mRNA expression when normalized against the DIO-only group (n = 3). *$P < 0.05$ is considered statistically significant. (B) qRT-PCR analysis of liver IL-1β, IL-12, IL-23, and Dectin-1 mRNA expression of MCS mice, MCD mice, and MCD mice treated with DETA NONOate for 4 weeks (MCD + NO). The y-axis represents the fold of mRNA expression when normalized against MCS-only group (n = 3). *$P < 0.05$ is considered statistically significant. (C) Analysis of IL-1β immunoreactivity (red) by immunofluorescence imaging of paraffin-embedded liver sections, counterstained with DAPI (blue) from (i) DIO, (ii) DIO + BDCM (1 week), (iii) DIO + BDCM + NO, (iv) MCS, (v) MCD, and (vi) MCD + NO. Magnification: 20× (n = 3). (D) Immunofluorescence images of IL-12 immunoreactivity (red) of paraffin-embedded liver sections counterstained with DAPI (blue) from (i) DIO, (ii) DIO + BDCM (1 week), (iii) DIO + BDCM + NO, (iv) MCS, (v) MCD, and (vi) MCD + NO. Magnification: 20× (n = 3).

showed that serum alanine aminotransferase levels and high-mobility group protein B1 mRNA expression were significantly decreased in the NO-donor administered groups as compared with the MCD or DIO + BDCM groups (Supplemental Figs. 1 and 2), which suggests that the marked decrease in CYP2E1 activity after NO donor administration decreases the bioactivation of BDCM and toxicity in MCD group.

NO Donor Administration Rescues Mice from NASH Progression. NASH progression is marked by a proinflammatory stage followed mostly by a fibrotic stage (Farrell and Larter, 2006; Bohinc and Diehl, 2012). Hepatic stellate cells transform into a more activated and proliferative phenotype (Mann and Marra, 2010; Bohinc and Diehl, 2012). There is increased collagen deposition and a buildup of extracellular matrix. If unchecked, this phenomenon can lead to scarring of the liver and ultimately can lead to liver cirrhosis (Ikejima et al., 2007). To study whether attenuation of M1 polarization by NO donor administration also rescued livers from the progressive NASH phenotype, we performed experiments in both models of NASH to study stellate cell proliferation and collagen deposition, and we performed histopathologic examinations of the affected livers using the NASH CRN (National Institutes of Health Nonalcoholic Steatohepatitis Clinical Research Network) scoring system.

Our results showed that administration of NO donor in both models of NASH significantly decreased the mRNA expression of α-SMA, a biomarker for stellate cell proliferation (Fig. 6, A and B) (*$P < 0.05$). The immunohistochemical analyses of liver slices from both the toxin and MCD models of NASH showed significant increased immunoreactivity of α-SMA in the sinusoidal regions of BDCM-treated NASH mice and MCD-diet mice (Fig. 6Ci and iii); there was decreased immunoreactivity for α-SMA in the NO-donor treated mice livers that were either in the toxin-administered group or in the MCD-diet group (Fig. 6Cii and iv). PicroSirius red staining for collagen deposition in the livers showed higher periportal fibrosis in both the toxin-treated mice and the MCD-diet mice,

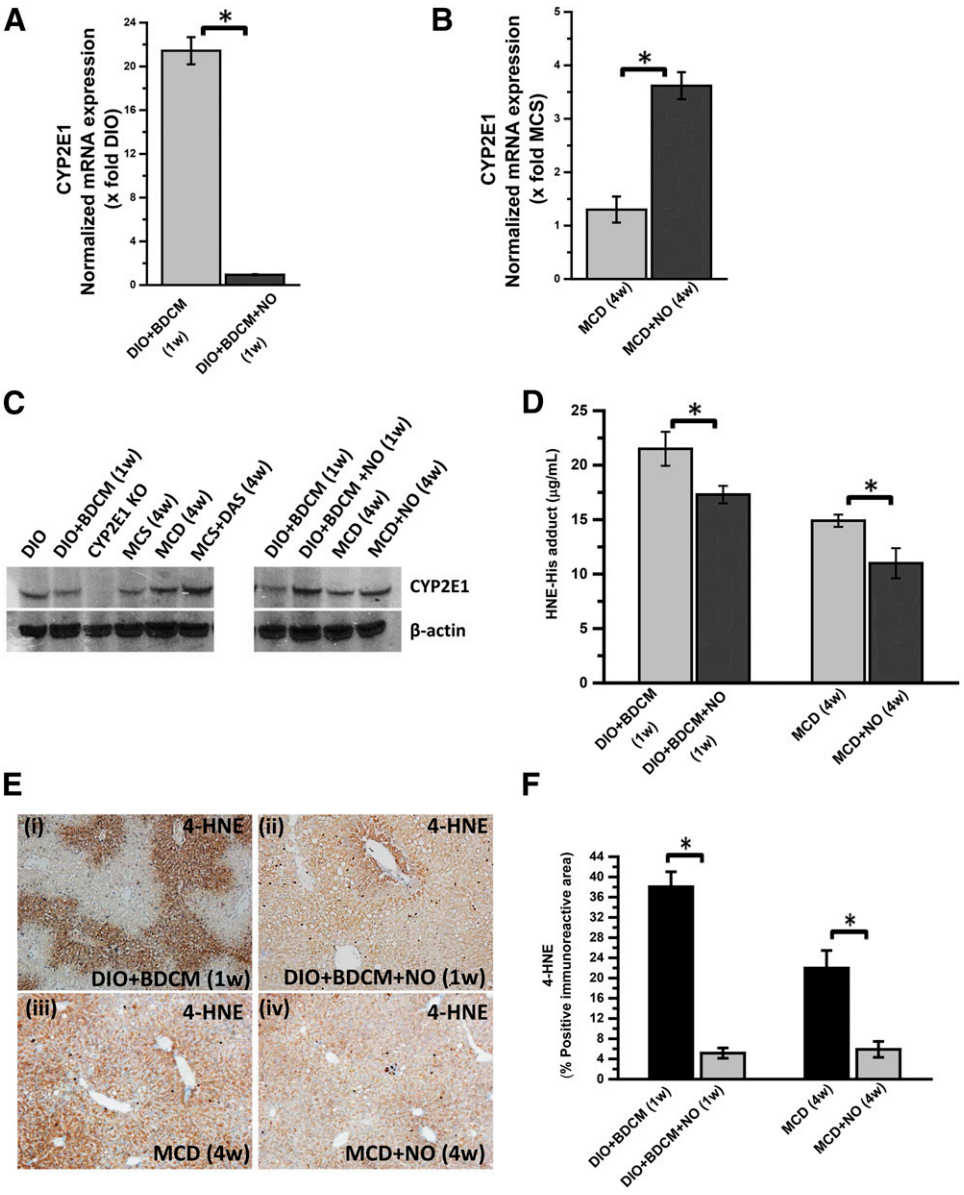

Fig. 5. NO donor (DETA NONOate) decreases oxidative stress by inhibiting CYP2E1 activity. (A) mRNA expression analysis of liver CYP2E1 by quantitative real-time polymerase chain reaction (qRT-PCR) of mice treated with DIO + BDCM (1 week) and DIO mice exposed to BDCM and treated with DETA NONOate for 1 week (DIO + BDCM + NO (1 week). The *y*-axis represents the fold of mRNA expression when normalized against the DIO-only group ($n = 3$). $^*P < 0.05$ is considered statistically significant. (B) qRT-PCR analysis of liver CYP2E1 mRNA expression of MCD mice and MCD mice treated with DETA NONOate for 4 weeks (MCD + NO). The *y*-axis represents the fold of mRNA expression when normalized against the MCS-only group ($n = 3$). $^*P < 0.05$ is considered statistically significant. (C) Western blot analysis of CYP2E1 protein expression levels in liver homogenates from the mice: DIO, DIO + BDCM (1 week), CYP2E1 KO, MCS, MCD, MCD + DAS, and DIO + BDCM (1 week), DIO + BDCM + NO (1 week), MCD (4 weeks), and MCD + NO (4 weeks). The corresponding β-actin levels are shown in the lower panel. (D) Quantification of 4-HNE-His adduct in mouse liver homogenate by indirect ELISA of mice treated with DIO + BDCM (1 week), DIO + BDCM + NO (1 week), MCD (4 weeks) and MCD + NO (4 weeks). The *y*-axis represents pg/mL of 4-HNE-His adduct ($n = 3$). $^*P < 0.05$ is considered statistically significant. (E) 4-HNE immunoreactivity analysis of mouse liver slices by immunohistochemical analysis depicting lipid peroxidation: DIO + BDCM (1 week), DIO + BDCM + NO (1 week), MCD (4 weeks), and MCD + NO (4 weeks). Magnification: 10× ($n = 3$). (F) Morphometric analysis of 4-HNE immunoreactivity. The *y*-axis shows the percentage of the positive immunoreactive area ($n = 3$), analysis performed on images from three separate microscopic fields. $^*P < 0.05$ is considered statistically significant.

but fibrosis was markedly reduced in the NO donor–treated mice (Fig. 6D).

Liver histology as evidenced by H&E staining showed decreased bipolar nuclei, infiltrating leukocytes, ballooning degeneration, and hepatocyte necrosis in the NO donor groups as compared with the BDCM-treated group (Fig. 6E). The NASH CRN scores showed a significant attenuation of the severity of NASH lesions (Fig. 6F). Thus, the results suggest that NO donor administration could significantly rescue mice from NASH lesions after NO donor administration throughout their entire period of high-fat diet, toxin exposure, or MCD diet feeding. A schematic representation of the NO-donor mechanism of action is provided in Fig. 7.

Discussion

In this study, we report for the first time a mechanistic investigation of oxidative stress-induced M1 polarization, evidenced by M1 cytokine release in NASH followed by a therapeutic intervention of the process by NO donor, which has an its inhibitory effect on CYP2E1, a vital enzyme with a recognized role in NASH progression. Our study found that lipid peroxidation-induced 4-HNE-His adducts that were generated from CYP2E1 catalysis of BDCM in the toxin model of NASH and the dietary oxidative stress in MCD model of NASH caused M1 polarization bias-induced cytokine release, including increased levels of the hepatic M1 markers IL-1β, IL-12, IL-23, and Dectin-1.

We used two distinct models of NASH progression in mice: 1) a specific ligand of CYP2E1 (BDCM) in an underlying condition of obesity (high-fat diet) and insulin resistance, and 2) a dietary model (MCD) where the mice progressed into steatohepatitis and fibrosis during oxidative stress, especially through CYP2E1, without obesity or insulin resistance. The use of these separate mouse models justified our approach of probing the involvement of oxidative stress M1 polarization-

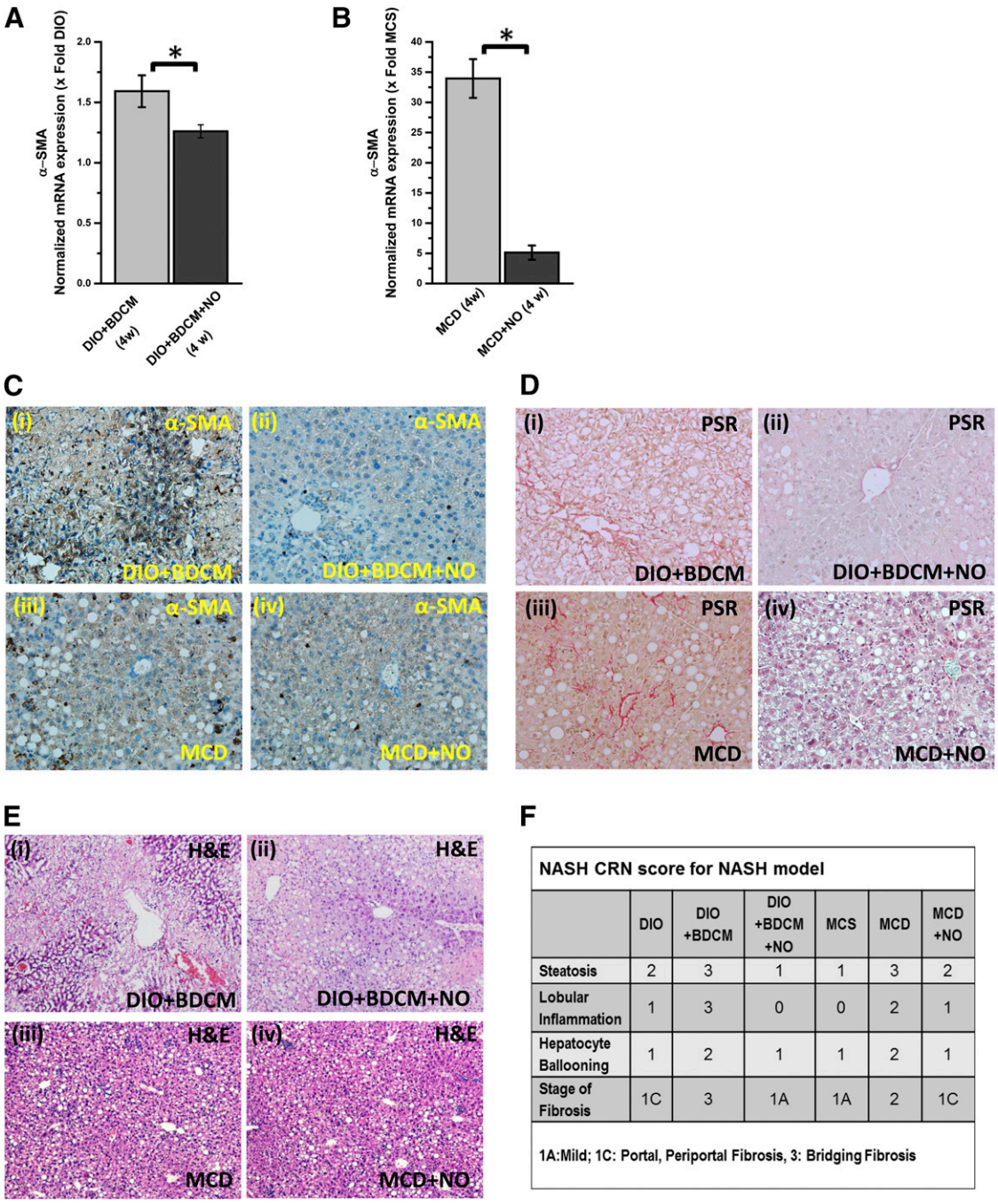

NASH CRN score for NASH model

	DIO	DIO +BDCM	DIO +BDCM +NO	MCS	MCD	MCD +NO
Steatosis	2	3	1	1	3	2
Lobular Inflammation	1	3	0	0	2	1
Hepatocyte Ballooning	1	2	1	1	2	1
Stage of Fibrosis	1C	3	1A	1A	2	1C

1A:Mild; 1C: Portal, Periportal Fibrosis, 3: Bridging Fibrosis

Fig. 6. NO donor (DETA NONOate) prevents NASH progression by inhibiting CYP2E1 activity and the resultant oxidative stress. (A) mRNA expression of liver α-SMA by quantitative real-time polymerase chain reaction (qRT-PCR) of DIO mice exposed to BDCM (DIO + BDCM) for 4 weeks, and DIO + BDCM mice treated with NO donor (DIO + BDCM + NO) for 4 weeks. The y-axis represents the fold of mRNA expression when normalized against the DIO-only group, $n = 3$. $^*P < 0.05$ is considered statistically significant. (B) qRT-PCR analysis of liver α-SMA mRNA expression of MCD mice and MCD mice treated with DETA NONOate (MCD + NO) for 4 weeks. The y-axis represents the fold of mRNA expression when normalized against the MCS-only group, $n = 3$. $^*P < 0.05$ is considered statistically significant. (C) The α-smooth muscle actin immunoreactivity as shown by immunohistochemistry in liver slices of (i) DIO mice exposed to BDCM; (ii) DIO + BDCM + NO; (iii) MCD mice, and (iv) MCD + NO. Magnification: 20× magnification ($n = 3$). (D) PicroSirius red staining of liver sections of (i) DIO mice exposed to BDCM; (ii) DIO + BDCM + NO; (iii) MCD mice, and (iv) MCD + NO. Magnification: 20× ($n = 3$). The red staining shows macrovesicular and microvesicular fibrosis. (E) H&E staining of liver sections of (i) DIO mice exposed to BDCM; (ii) DIO + BDCM + NO; (iii) MCD mice, and (iv) MCD + NO. Magnification: 10× ($n = 3$). (F) Stained liver sections were reviewed for stages of fibrosis using the criteria of the NIH Non Alcoholic Steatohepatitis Clinical Research Network (NIH NASH CRN). The table depicts the NASH CRN scores for DIO, DIO + BDCM, DIO + BDCM + NO, MCS, MCD, and MCD + NO.

induced cytokine release without having to limit our interpretation to a single dietary model of NASH.

We previously showed that BDCM exposure in mice fed a high-fat diet caused NASH (Das et al., 2013a; Seth et al., 2013). These mice had an increased proinflammatory cytokine release (at 1 week) followed by a progressive fibrotic stage (up to 4 weeks). The increased proinflammatory phase was primarily related to CYP2E1-mediated oxidative stress and

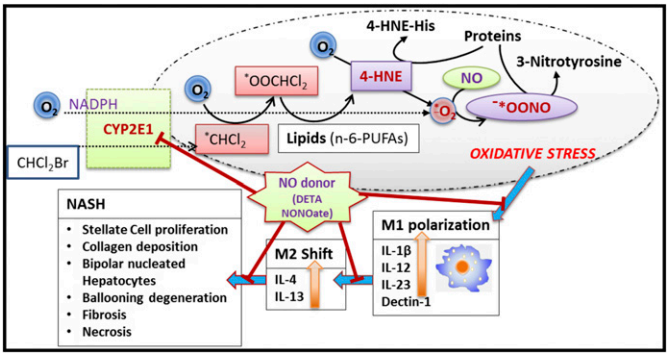

Fig. 7. Schematic representation of the study. The graphics scheme shows the proposed mechanism of action of DETA NONOate. The red lines represent the checkpoints where the drug can have its potential inhibitory role.

inflammosome activation due to priming of P2X7r (Das et al., 2013b). Others have studied T_H1 polarization in NASH in detail (Ferreyra Solari et al., 2012; Maina et al., 2012; Sutti et al., 2014). The higher incidence of interferon-γ release is primarily from a heightened T_H1 response and is found to be due to oxidative stress–mediated malonyldialdehyde adducts that elicit a strong autoantibody response (Sutti et al., 2014). The adaptive immune response, then, is responsible for macrophage polarization mainly through the M1 phenotype (Sutti et al., 2014).

Our observation of decreased hepatic M1 markers in CYP2E1-null mice and in mice treated with the CYP2E1 inhibitor DAS in both models of NASH indicates a close association of CYP2E1-induced oxidative stress in causing M1 polarization bias and an increase in M1 markers. Importantly, our approach to depleting macrophages by using $GdCl_3$ in the liver was based on identifying the precise origin of the inflammatory cytokines, especially IL-1β, IL-12, IL-23, and Dectin-1; we were well aware that IL-1β release has other cellular sources in the liver as well. Our results with CYP2E1-mediated M1 polarization in NASH provide insight into the mechanisms of macrophage responses, which had been scarce aside from a few isolated studies where morbidly obese patients with NASH etiology were shown to produce increased T_H1 cytokines and Kupffer cell responses (Fukushima et al., 2009; Bertola et al., 2010; Bieghs et al., 2013). There has been preclinical evidence for the involvement of Kupffer cells with an M1 phenotype, the former being responsible for NASH progression, but those studies did not clarify the role of oxidative stress, especially mediated by CYP2E1, in causing a M1 polarization bias (Fukushima et al., 2009; Bieghs et al., 2013).

Important from the mechanistic point of view, we observed an increase in hepatic NO levels in the diet + toxin NASH model. NO, released from any of the three NOS upon their activation, plays a significant role in inflammation (Fujita et al., 2010; Ajamieh et al., 2012). However, the inducible form of the NOS has been ascribed to the proinflammatory phenotype more often (Fujita et al., 2010; Maina et al., 2012). Our results showed that NO levels reached a 4-fold increase as early as 24 hours after coexposure with diet and toxin to induce NASH, and they stayed at the same level for the entire study period. Early use of 1400W decreased the NO levels. Interestingly, the use of NOS2-null mice at a late stage (4 weeks) did not affect the NO levels in NASH, suggesting that other NOS isoforms, especially NOS3 might be involved in the sustained higher NO levels at the late stage in our study. Moreover, the observed increase in NO may be an adaptive response of the injured liver. Ajamieh et al. (2012) found that there were increases in NOS3 levels and NOS3 phosphorylations after liver injury in NASH, and they were found to be protective against NASH. Based on these observations, we argued that though NO is considered proinflammatory and an M1 marker, the kinetics of NO release and its concentration in the hepatic microenvironment might play an adaptive and perhaps a protective role in the pathophysiology of NASH.

To alter the NO levels we used a dual approach. We used NOS2-null mice and a nonspecific inhibitor of NOS. Subsequently, we used an NO donor DETA NONOate for administration through the intraperitoneal route to increase the in vivo concentration of NO, assuming that the increase in NO was an adaptive response to the liver injury. Although blocking NO synthase did not change the levels of M1 polarization markers or NASH symptoms (data not shown), treatment with an NO donor significantly lowered levels of both mRNA and protein expressions of M1 markers in the toxin model but only protein levels in the MCD model of NASH (Fig. 4, A–D), suggesting the existence of a plausible mechanism for NO-mediated suppression of proinflammatory events in early NASH developmental stages.

Having identified an association of CYP2E1-induced oxidative stress as a mediator in M1 polarization, we studied the role of a late M2 phenotype that might cause fibrosis, a feature that is of paramount importance in the human form of the disease. Results from our studies showed that mice with high-fat diet–induced obesity and with coexposure to the toxin BDCM had increased mRNA and protein expressions of the prominent M2 markers IL-4 and IL-13; however, the mice that were pretreated with the macrophage toxin $GdCl_3$ did not show the IL-4 and IL-13 increases, suggesting that the macrophage origin contributed at least partly to the M2 phenotypic shift in the late stage of the disease. Because the NO donor prevented M1 polarization bias, we also would argue that a higher NO concentration from the initial phases of disease development might resist the proinflammatory events in early stages of NASH, with a corresponding decrease in the M2 phenotypic response, thus attenuating NASH progression.

Because M1 polarization was associated with CYP2E1-mediated oxidative stress and CYP2E1 activity is strongly inhibited by NO, we studied the role of NO donor (DETA NONOate) in abrogating oxidative stress, mediated by CYP2E1 activity. Our findings of a strong inhibition of 4-HNE-His adducts in both the models of NASH were in complete agreement with the pioneering study by Gergel et al. (1997), who showed that CYP2E1 catalytic activity and reactive oxygen radical formation were inhibited by NO (Fig. 5). Our observation that there was no change in the CYP2E1 protein level after NO donor administration also confirmed that the NO donor inhibited CYP2E1 activity in the in vivo system we used for our study.

NASH pathophysiology is associated with stellate cell proliferation, fibrosis, and hepatocellular necrosis (Bohinc and Diehl, 2012; Seth et al., 2013). NO donor administration significantly decreased stellate cell proliferation, as evidenced by the decreased α-SMA protein levels, and decreased

hepatocellular necrosis, inflammation, and fibrosis, as shown by the NASH CRN scores (Fig. 6). Thus, taken together, this study showed that oxidative stress mediated by CYP2E1 induced M1 polarization-induced cytokines, which, in tur,n may have been responsible for late anti-inflammatory events that resulted in fibrosis. Mechanistically, administration of NO donor that increased the NO levels in the liver significantly (6.6-fold as compared with 3.4-fold; data not shown) could block CYP2E1 activity and the subsequent inflammatory events that lead to NASH pathophysiology. Our study offers a therapeutic approach through the use of NO donors as prospective drugs for NASH treatment and leads the way to more detailed insight into developing newer effective pharmacologic strategies involving synthetic NO donors with longer half-lives to contain NASH-related comorbidities.

Acknowledgments

The authors thank Benny Davidson at the Instrumentation Resource Facility (IRF), University of South Carolina School of Medicine for technical services. The authors also thank Dr. James Carson, Department of Exercise Science and the IRF at the University of South Carolina for equipment usage and consulting services.

Authorship Contributions

Participated in research design: Chatterjee, Seth.

Conducted experiments: Seth, Das, Pourhosseini, Dattaroy, Igwe.

Contributed new reagents or analytic tools: Diehl, Michelotti.

Performed data analysis: Chatterjee, Das, Seth.

Wrote or contributed to the writing of the manuscript: Chatterjee, Fan, Diehl, Basu-Ray, Michelotti.

References

Abdelmegeed MA, Banerjee A, Jang S, Yoo SH, Yun JW, Gonzalez FJ, Keshavarzian A, and Song BJ (2013) CYP2E1 potentiates binge alcohol-induced gut leakiness, steatohepatitis, and apoptosis. *Free Radic Biol Med* **65**:1238–1245.

Abdelmegeed MA, Banerjee A, Yoo SH, Jang S, Gonzalez FJ, and Song BJ (2012) Critical role of cytochrome P450 2E1 (CYP2E1) in the development of high fat-induced non-alcoholic steatohepatitis. *J Hepatol* **57**:860–866.

Aitken AE, Lee CM, and Morgan ET (2008) Roles of nitric oxide in inflammatory downregulation of human cytochromes P450. *Free Radic Biol Med* **44**:1161–1168.

Ajamieh H, Farrell G, Wong HJ, Yu J, Chu E, Chen J, and Teoh N (2012) Atorvastatin protects obese mice against hepatic ischemia-reperfusion injury by Toll-like receptor-4 suppression and endothelial nitric oxide synthase activation. *J Gastroenterol Hepatol* **27**:1353–1361.

Aubert J, Begriche K, Knockaert L, Robin MA, and Fromenty B (2011) Increased expression of cytochrome P450 2E1 in nonalcoholic fatty liver disease: mechanisms and pathophysiological role. *Clin Res Hepatol Gastroenterol* **35**:630–637.

Bertola A, Bonnafous S, Anty R, Patouraux S, Saint-Paul MC, Iannelli A, Gugenheim J, Barr J, Mato JM, and Le Marchand-Brustel Y, et al. (2010) Hepatic expression patterns of inflammatory and immune response genes associated with obesity and NASH in morbidly obese patients. *PLoS ONE* **5**:e13577.

Bieghs V, Walenbergh SM, Hendrikx T, van Gorp PJ, Verheyen F, Olde Damink SW, Masclee AA, Koek GH, Hofker MH, and Binder CJ, et al. (2013) Trapping of oxidized LDL in lysosomes of Kupffer cells is a trigger for hepatic inflammation. *Liver Int* **33**:1056–1061.

Bohinc BN and Diehl AM (2012) Mechanisms of disease progression in NASH: new paradigms. *Clin Liver Dis* **16**:549–565.

Caro AA and Cederbaum AI (2004) Oxidative stress, toxicology, and pharmacology of CYP2E1. *Annu Rev Pharmacol Toxicol* **44**:27–42.

Chatterjee S, Ehrenshaft M, Bhattacharjee S, Deterding LJ, Bonini MG, Corbett J, Kadiiska MB, Tomer KB, and Mason RP (2009) Immuno-spin trapping of a post-translational carboxypeptidase B1 radical formed by a dual role of xanthine oxidase and endothelial nitric oxide synthase in acute septic mice. *Free Radic Biol Med* **46**:454–461.

Chatterjee S, Ganini D, Tokar EJ, Kumar A, Das S, Corbett J, Kadiiska M, Waalkes M, Diehl AM, and Mason RP (2013) Leptin is key to peroxynitrite-mediated oxidative stress and Kupffer cell activation in experimental non-alcoholic steatohepatitis. *J Hepatol* **58**:778–784.

Chatterjee S, Premachandran S, Bagewadikar RS, Bhattacharya S, Chattopadhyay S, and Poduval TB (2006) Arginine metabolic pathways determine its therapeutic benefit in experimental heatstroke: role of Th1/Th2 cytokine balance. *Nitric Oxide* **15**:408–416.

Cheung O and Sanyal AJ (2009) Recent advances in nonalcoholic fatty liver disease. *Curr Opin Gastroenterol* **25**:230–237.

Copaci I, Micu L, and Voiculescu M (2006) The role of cytokines in non-alcoholic steatohepatitis. A review. *J Gastrointestin Liver Dis* **15**:363–373.

Das S, Kumar A, Seth RK, Tokar EJ, Kadiiska MB, Waalkes MP, Mason RP, and Chatterjee S (2013a) Proinflammatory adipokine leptin mediates disinfection byproduct bromodichloromethane-induced early steatohepatitic injury in obesity. *Toxicol Appl Pharmacol* **269**:297–306.

Das S, Seth RK, Kumar A, Kadiiska MB, Michelotti G, Diehl AM, and Chatterjee S (2013b) Purinergic receptor X7 is a key modulator of metabolic oxidative stress-mediated autophagy and inflammation in experimental nonalcoholic steatohepatitis. *Am J Physiol Gastrointest Liver Physiol* **305**:G950–G963.

de Oliveira CP, de Lima VM, Simplicio FI, Soriano FG, de Mello ES, de Souza HP, Alves VA, Laurindo FR, Carrilho FJ, and de Oliveira MG (2008) Prevention and reversion of nonalcoholic steatohepatitis in OB/OB mice by S-nitroso-N-acetylcysteine treatment. *J Am Coll Nutr* **27**:299–305.

Farrell GC and Larter CZ (2006) Nonalcoholic fatty liver disease: from steatosis to cirrhosis. *Hepatology* **43**(2, Suppl 1)S99–S112.

Ferreyra Solari NE, Inzaugarat ME, Baz P, De Matteo E, Lezama C, Galoppo M, Galoppo C, and Cherñavsky AC (2012) The role of innate cells is coupled to a Th1-polarized immune response in pediatric nonalcoholic steatohepatitis. *J Clin Immunol* **32**:611–621.

Fujita K, Nozaki Y, Yoneda M, Wada K, Takahashi H, Kirikoshi H, Inamori M, Saito S, Iwasaki T, and Terauchi Y, et al. (2010) Nitric oxide plays a crucial role in the development/progression of nonalcoholic steatohepatitis in the choline-deficient, l-amino acid-defined diet-fed rat model. *Alcohol Clin Exp Res* **34** (Suppl 1):S18–S24.

Fukushima J, Kamada Y, Matsumoto H, Yoshida Y, Ezaki H, Takemura T, Saji Y, Igura T, Tsutsui S, and Kihara S, et al. (2009) Adiponectin prevents progression of steatohepatitis in mice by regulating oxidative stress and Kupffer cell phenotype polarization. *Hepatol Res* **39**:724–738.

Ganz M and Szabo G (2013) Immune and inflammatory pathways in NASH. *Hepatol Int* **7**:771–781.

Gergel D, Misík V, Riesz P, and Cederbaum AI (1997) Inhibition of rat and human cytochrome P4502E1 catalytic activity and reactive oxygen radical formation by nitric oxide. *Arch Biochem Biophys* **337**:239–250.

Gong P, Cederbaum AI, and Nieto N (2004) The liver-selective nitric oxide donor O2-vinyl 1-(pyrrolidin-1-yl)diazen-1-ium-1,2-diolate (V-PYRRO/NO) protects HepG2 cells against cytochrome P450 2E1-dependent toxicity. *Mol Pharmacol* **65**:130–138.

Hu JJ, Yoo JS, Lin M, Wang EJ, and Yang CS (1996) Protective effects of diallyl sulfide on acetaminophen-induced toxicities. *Food Chem Toxicol* **34**:963–969.

Ikejima K, Okumura K, Kon K, Takei Y, and Sato N (2007) Role of adipocytokines in hepatic fibrogenesis. *J Gastroenterol Hepatol* **22** (Suppl 1):S87–S92.

Liu YC, Zou XB, Chai YF, and Yao YM (2014) Macrophage polarization in inflammatory diseases. *Int J Biol Sci* **10**:520–529.

Maina V, Sutti S, Locatelli I, Vidali M, Mombello C, Bozzola C, and Albano E (2012) Bias in macrophage activation pattern influences non-alcoholic steatohepatitis (NASH) in mice. *Clin Sci (Lond)* **122**:545–553.

Mann DA and Marra F (2010) Fibrogenic signalling in hepatic stellate cells. *J Hepatol* **52**:949–950.

Pasarín M, La Mura V, Gracia-Sancho J, García-Calderó H, Rodríguez-Vilarrupla A, García-Pagán JC, Bosch J, and Abraldes JG (2012) Sinusoidal endothelial dysfunction precedes inflammation and fibrosis in a model of NAFLD. *PLoS ONE* **7**:e32785.

Seth RK, Das S, Kumar A, Chanda A, Kadiiska MB, Michelotti G, Manautou J, Diehl AM, and Chatterjee S (2014) CYP2E1-dependent and leptin-mediated hepatic CD57 expression on CD8+ T cells aid progression of environment-linked non-alcoholic steatohepatitis. *Toxicol Appl Pharmacol* **274**:42–54.

Seth RK, Kumar A, Das S, Kadiiska MB, Michelotti G, Diehl AM, and Chatterjee S (2013) Environmental toxin-linked nonalcoholic steatohepatitis and hepatic metabolic reprogramming in obese mice. *Toxicol Sci* **134**:291–303.

Shimamura T, Fujisawa T, Husain SR, Kioi M, Nakajima A, and Puri RK (2008) Novel role of IL-13 in fibrosis induced by nonalcoholic steatohepatitis and its amelioration by IL-13R-directed cytotoxin in a rat model. *J Immunol* **181**: 4656–4665.

Sutti S, Jindal A, Locatelli I, Vacchiano M, Gigliotti L, Bozzola C, and Albano E (2014) Adaptive immune responses triggered by oxidative stress contribute to hepatic inflammation in NASH. *Hepatology* **59**:886–897.

Tilg H and Moschen AR (2008) Inflammatory mechanisms in the regulation of insulin resistance. *Mol Med* **14**:222–231.

Tilg H and Moschen AR (2010) Evolution of inflammation in nonalcoholic fatty liver disease: the multiple parallel hits hypothesis. *Hepatology* **52**:1836–1846.

Tomasi A, Albano E, Biasi F, Slater TF, Vannini V, and Dianzani MU (1985) Activation of chloroform and related trihalomethanes to free radical intermediates in isolated hepatocytes and in the rat in vivo as detected by the ESR-spin trapping technique. *Chem Biol Interact* **55**:303–316.

Whitsett J, Picklo MJ, Sr, and Vasquez-Vivar J (2007) 4-Hydroxy-2-nonenal increases superoxide anion radical in endothelial cells via stimulated GTP cyclohydrolase proteasomal degradation. *Arterioscler Thromb Vasc Biol* **27**:2340–2347.

Zhou D, Kong L, Zhou Q, and Li J (2014) Skewing KC phenotypic polarization into M2 via the intervention of oxidized LDL as potential therapeutic implications for NASH. *Liver Int* **34**:815–816.

Address correspondence to: Dr. Saurabh Chatterjee, Environmental Health and Disease Laboratory, Department of Environmental Health Sciences, University of South Carolina, Columbia, SC 29208. E-mail: schatt@mailbox.sc.edu